



Disorder in the chalcogen layer in $1T$ -TaS_{2-x}Se_xSharon S. Philip and Despina Louca 
University of Virginia, Charlottesville, Virginia 22904, USA (Received 22 September 2023; revised 28 November 2023; accepted 1 March 2024; published 26 March 2024)

The charge density wave (CDW) system $1T$ -TaS_{2-x}Se_x was investigated using neutron scattering to determine the nature of the in-plane and out-of-plane disorder. From the local structure analysis, it was deduced that the in-plane star of David motifs are distorted with Se doping just like it was previously observed in $1T$ -TaS₂. This is due to random Ta displacements away from the ideal trigonal symmetry regardless of whether the CDW state is commensurate, nearly commensurate, metallic, or insulating. In the chalcogen layer, the atoms are also distorted with displacements in the perpendicular direction to the planes. The chalcogen distortions are most pronounced in TaS₂ that superconducts below 3.6 K in comparison to the distortions observed in TaS₂ and TaSe₂. The implications of the distortions on superconductivity and the effects on the electron pocket proposed to lead to the superconducting state are not understood at present. Unlike in $1T$ -TaS₂ in which both 13c and 3c layer stacking orders were previously reported, in the nearly commensurate metallic state of $1T$ -TaS₂ and the commensurate CDW metallic state of TaSe₂, no clear evidence for a stacking order is observed down to 2 K.

DOI: [10.1103/PhysRevB.109.094118](https://doi.org/10.1103/PhysRevB.109.094118)**I. INTRODUCTION**

Lattice distortions intrinsically control the behavior, and hence the utility, of electronic materials serving in a wide array of applications [1–5]. Quasi-two-dimensional (2D) transition metal dichalcogenides (TMDs) are prone to electronic instabilities, exhibiting incredibly rich phase diagrams with emergent behaviors [6–8]. TMDs are important in a broad scientific area and can find their way in many technologies because of their tunable characteristics. Constructed on simple stacking principles, layers of transition metal alternate with the chalcogen ion [9,10]. TMD $1T$ -TaS_{2-x}Se_x is a prototype charge density wave (CDW) system where a cooperative periodic modulation of the charge density and the crystal structure, coupled with Mott-insulating and superconducting phases, propagates across the entire phase diagram [11,12]. Moreover, $1T$ -TaS₂ is a quantum spin liquid candidate as well, which is a highly entangled state [13,14]. With doping, three main phases appear: the incommensurate CDW (ICDW), the nearly commensurate CDW (NCCDW), and the commensurate CDW (CCDW) [15]. The ICDW state is metallic and appears below 540 K upon cooling from the high-temperature metallic state. Coupled with this is a transition from the $P\bar{3}m1$ crystal symmetry shown in Fig. 1(a) to the $P\bar{3}$ structure [16–18]. This transition is driven by the Ta displacements that yield the well-known star of David motifs. A typical star lattice within the CDW supercell is shown in Fig. 1(b).

In the ICDW state, the stars do not order in-plane. Cooling leads to the ICDW state becoming the NCCDW state, where the $\sqrt{13} \cdot \sqrt{13}$ structural modulation appears with a 12° tilt relative to the original *ab* plane. An expansion of the star of David lattice occurs in-plane [16]. At the two ends of the phase diagram, the $\sqrt{13} \cdot \sqrt{13}$ structural modulation persists with a rotation of 13.9° as it enters the CCDW state. On the other hand, in the middle of the phase diagram, the NCCDW state persists [15]. It is in this region that superconductivity

emerges upon doping that coexists with the broad NCCDW region as shown in the phase diagram by Ref. [15]. In this work, we explore features in the local structure that are preserved across phase boundaries through isovalent doping, and we search for variations in the local parameters that control the crossover mechanism giving rise to the different states. In addition, we search for stacking order as a function of doping. Previously, in $1T$ -TaS₂, 13c as well as 3c layer stacking types were observed as shown in Fig. 1(c). It is conceivable that it is this layer stacking that drives the insulating transition [19,20].

Superconductivity emerges in $1T$ -TaS₂ in a number of different ways, such as by applying high pressure [6], by introducing disorders in the crystal [7], and by substitutions made at the Ta atom and S atom sites [8,21]. It has been reported that the substitution of S with Se in $1T$ -TaS_{2-x}Se_x induces superconductivity in the doping concentration $0.8 \leq x \leq 1.6$ [15,21] with a maximum superconducting onset temperature of 3.6 K at $x = 1$ is shown in Fig. 1(d). The interplay between CDW order and superconductivity has been investigated in many different dichalcogenide systems. Nonetheless, questions remain regarding the role of disorder and its implications in the cooperative CDW state. The entanglement of CDW with superconductivity is probed using neutron scattering and the pair density function (PDF) analysis technique. Previously, we observed a hysteresis in the local structure between cooling and warming in $1T$ -TaS₂ that couples to the hysteresis observed in the resistivity during the CCDW-NCCDW transition [22]. The observation of the local structural anomaly coupled to the hysteresis in resistivity suggests a strong electron-lattice coupling [22] in addition to the already observed structural modulation with the $\sqrt{13} \cdot \sqrt{13}$ pattern. In fact, the $\sqrt{13} \cdot \sqrt{13}$ pattern does not change across the CCDW-NCCDW transition; hence, the observed local disorder of the stars couples directly to this transition. This finding may have significant implications towards understanding the phenomenon of CDW modulations and local correlations in this

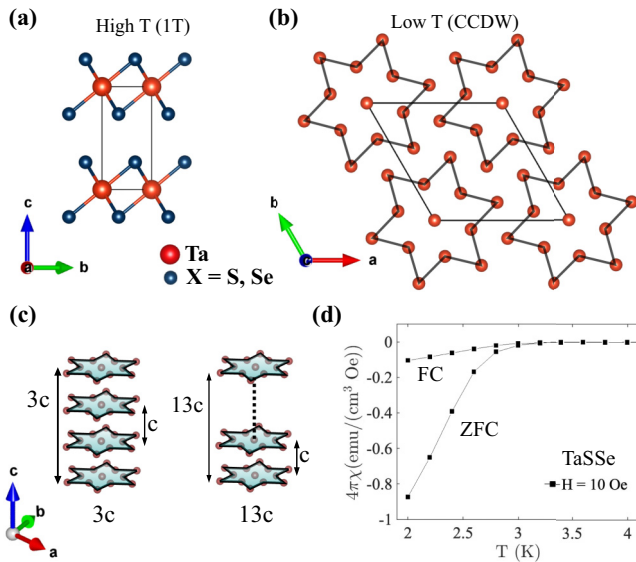


FIG. 1. (a) The unit cell of the high-temperature phase of $1T\text{-TaX}_2$ with the $P\bar{3}m1$ structure. (b) Below the CDW transition, in-plane and out-of-plane modulations are present. The $\sqrt{13} \cdot \sqrt{13}$ supercell in the CCDW phase gives rise to the star lattice. (c) A schematic for the 13c and 3c stacking orders. (d) The low-temperature DC magnetic susceptibility of $1T\text{-TaS}_2$ showing the superconducting transition.

class of materials. In the present work, we investigated the out-of-plane layer stacking and the in-plane local structures in bulk samples of Se-doped $1T\text{-TaS}_{2-x}\text{Se}_x$ from room temperature and below. $1T\text{-TaSe}_2$ and $1T\text{-TaS}_2$ are isostructural to $1T\text{-TaS}_2$ and form the $\sqrt{13} \cdot \sqrt{13}$ superlattice. $1T\text{-TaSe}_2$ goes from the ICDW phase to the CCDW phase at 473 K directly without going through an intermediate NCCDW state. On the other hand, $1T\text{-TaS}_2$ goes from ICDW to NCCDW without entering a CCDW state. This sample is superconducting as shown in Fig. 1(d). With doping, it is observed that the local star-of-David lattice is equally distorted in-plane as in pristine $1T\text{-TaS}_2$. At the same time, from the diffraction studies, no definitive evidence of a 13c or 3c layer stacking order has been identified in $1T\text{-TaS}_2$ or $1T\text{-TaSe}_2$.

II. MATERIALS AND METHODS

Powders of TaSe_2 and TaS_2 were prepared using a solid-state reaction. Neutron powder diffraction measurements were performed to investigate the nature of the structure correlations in the CCDW and NCCDW phases. The time-of-flight neutron measurements were carried out at the Nanoscale Ordered Materials Diffractometer (NOMAD/BL-1B) and SEQUOIA (BL-17), a direct geometry spectrometer, at the Spallation Neutron Source of Oak Ridge National Laboratory at temperatures ranging from 2 to 300 K. An aluminium can was used for the SEQUOIA measurements and the empty can was subtracted from the data. The diffraction data from NOMAD were collected using a vanadium can and the data were used for the Rietveld refinement that provides the structural parameters for the periodic unit cell [23]. Preferred orientation effects were considered in the Rietveld refinement and were

not significant. The same data were used for the PDF analysis that provides information on the local arrangement of atoms. The PDF analysis provides a real-space representation of the local atomic correlations without assuming lattice periodicity. Using the NOMAD data, the total structure function $S(Q)$ was obtained as a function of the momentum transfer Q . The $S(Q)$ was Fourier transformed into real space to obtain the $G(r)$ [24,25]. The instrument background and empty sample can were subtracted from the $S(Q)$ and the data were normalized by vanadium. A maximum Q of 40 \AA^{-1} was used. The $G(r)$ is a function of the probability of finding a particular pair of atoms with an interatomic distance r [25].

III. RESULTS AND DISCUSSION

The Ta-based TMDs exhibit various polytypes based on the arrangement of the transition metal and chalcogen ions along the c axis. In this work, we focus on the $1T$ polytype of TaX_2 ($X = \text{S}$ or Se) with a hexagonal structure where the Ta atoms are octahedrally coordinated with six X atoms. The Ta atoms are sandwiched between X atom layers and the TaX_2 layers are held together by weak van der Waals forces leading to the quasi-2D nature. The unit cell with $P\bar{3}m1$ crystal symmetry is shown in Fig. 1(a) for the $1T$ phase. This is the high-temperature crystal symmetry that is associated with the $1T$ normal state of $1T\text{-TaX}_2$, above the ICDW transition. Upon cooling through the multiple CDW steps that $1T\text{-TaS}_2$ is known for, periodic lattice distortions form an in-plane $\sqrt{13} \cdot \sqrt{13}$ superlattice. The star-of-David forms when 12 Ta atoms displace towards a central Ta atom, producing stars at the corners of the trigonal unit cell [Fig. 1(b)]. The crystal structure below the ICDW transition is identified to be in the $P\bar{3}$ symmetry, and this symmetry persists through the multiple transitions observed upon cooling. The star lattice expands to form a commensurate structure continuously through the multiple CDW transitions, across the phase boundaries, and no sharp changes occur in the structure at the temperatures corresponding to the kinks observed in the transport [22,26].

The crystal symmetry remains the same across the phase diagram with Se doping. This is observed in the refinement of the neutron diffraction data collected at 2 K for TaS_2 and TaSe_2 shown in Figs. 2(a) and 2(b), respectively, from NOMAD. The average model with $P\bar{3}$ symmetry agrees well with both data sets, and the goodness of fit R_w values were calculated to be 0.073 for TaS_2 and 0.067 for TaSe_2 . These values are comparable to the agreement seen in TaS_2 as reported in Ref. [22]. The lattice constants show typical thermal expansion behavior [27]. Evidence for a layer stacking order was clearly observed in the Mott-insulating $1T\text{-TaS}_2$ [27]. Previously, we identified two types of stacking order, 13c and 3c. A schematic for these two is shown in Fig. 1(c). The CDW phase is characterized by multiple satellite peaks corresponding to the superstructure reflections [22]. With doping, however, it is not clear whether these stacking ordering schemes survive. Both TaS_2 and TaSe_2 were measured at SEQUOIA and no evidence for the kind of superlattice reflections in response to stacking order seen in TaS_2 was observed. Further single-crystal measurements are under way in search of evidence of stacking.

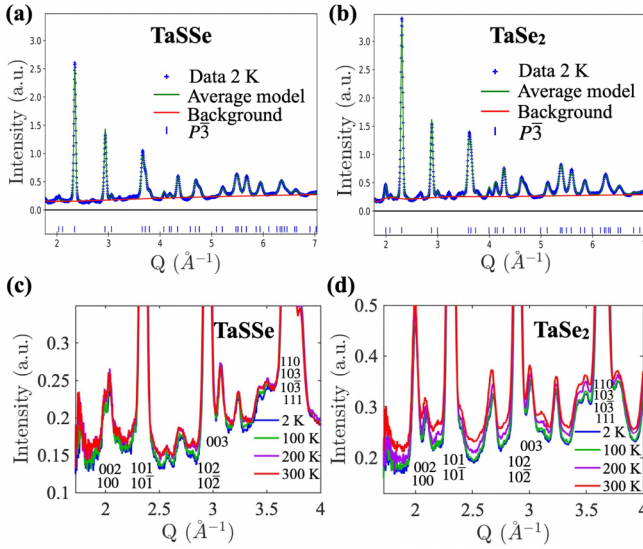


FIG. 2. The powder neutron diffraction results from NOMAD. The structure function at 2 K for (a) TaSSe and (b) TaSe₂ are shown. The data are compared to the average structure model with $P\bar{3}$ symmetry. The temperature dependence of the powder diffraction data in the low- Q region for (c) TaSSe and (d) TaSe₂ are shown. The Bragg peaks are labeled as shown.

As a function of temperature, the diffraction patterns for TaSSe and TaSe₂ change in the way shown in Figs. 2(c) and 2(d). Some of the Bragg peaks are labeled. No evidence of a structural change is observed.

The temperature dependence of the local structures for TaSSe and TaSe₂ is shown in Figs. 3(a) and 3(b), respectively. The $G(r)$'s were determined using the neutron diffraction data collected upon warming from 2 to 300 K on NOMAD. In

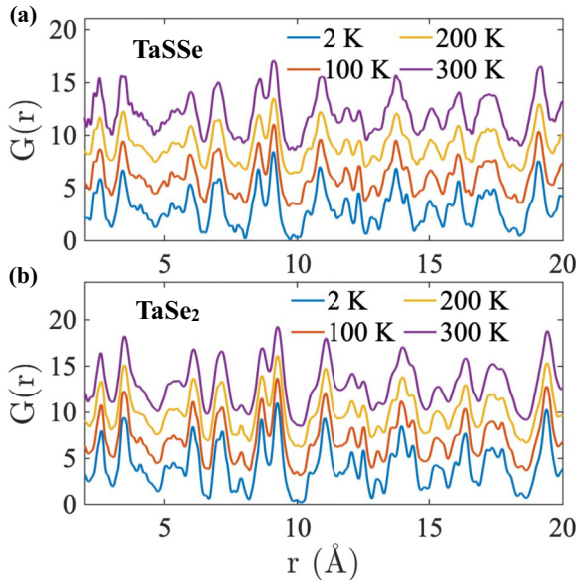


FIG. 3. The temperature dependence of the $G(r)$'s corresponding to the local structures of (a) TaSSe and (b) TaSe₂. No distinctive new features appear as a function of temperature, which indicates the absence of any phase transition in the measured temperature range.

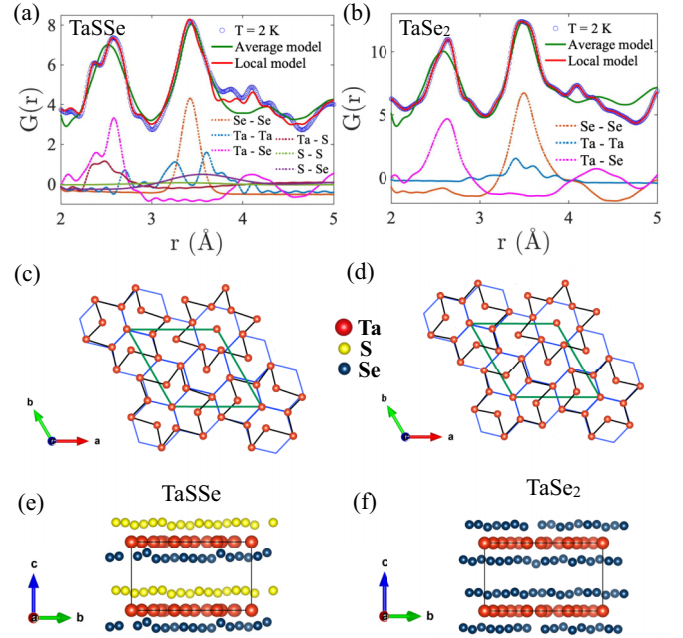


FIG. 4. The experimental neutron PDF data at 2 K compared with the calculated PDF based on the average model and the local model for (a) TaSSe and (b) TaSe₂. The partial PDFs describing the individual atom pair correlations are shown as well. The in-plane [panels (c) and (d)] and the out-of-plane [panels (e) and (f)] local models for these systems showing the distorted star of David structures within the CDW superlattice at 2 K. The in-plane model shows one superlattice unit cell where distorted stars are centered at the Ta atoms on the corners of the unit cell. The blue hexagons are shown to represent the Ta atom positions in the absence of any distortions.

TaSSe, the transition from the ICDW state to the NCCDW state occurs at ≈ 350 K. Thus, all the data shown are in the NCCDW state. The local structure shows some small changes across temperature that can be accounted for by thermal effects. Similarly, in TaSe₂ shown in Fig. 3(b), the ICDW to CCDW transition occurs around 500 K, with no intermediate phase and no insulating state either as observed in TaS₂. Locally, the atomic structure changes very little within the given temperature range. $G(r)$ for longer r range for both TaSSe and TaSe₂ is given in Supplemental Material [28].

The local atomic structure of 1T-TaSSe at 2 K is shown in Fig. 4(a) where the experimental $G(r)$ is compared to two models. The first model is calculated using the periodic cell with the $\sqrt{13} \cdot \sqrt{13}$ structural modulation shown in Fig. 1(b). The calculated $G(r)$ based on this average model is plotted with a green solid line. Clear differences are observed between this model and the experimental PDF, which indicate that the local structure is distorted beyond what the periodic star lattice can account for. Note how the average model does not reproduce the pair correlations that appear around 4 Å. The second model shown in the figure is calculated by lowering the symmetry to $P1$ and allowing all atom positions to refine to best fit the data. This model considers S and Se atoms to be in alternate planes ($z = 0.25$ and 0.75 , respectively). The calculated $G(r)$ based on this local model is plotted with a red solid line. Also shown in this figure are the calculated partials from the local model. From this we can see that the first set

of peaks corresponds to Ta-S and Ta-Se bond correlations. The second set of peaks corresponds to a double Ta-Ta peak, in addition to Se-Se and S-S correlations. It is interesting to note that there is only a single peak for the Se-Se and S-S correlations, which indicates that the in-plane Se-Se and S-S correlations are uniform. On the other hand, the Ta-Ta correlations indicate that the Ta in-plane correlations are split. Thus, the local correlations in the data around 4 Å mostly arise from new bond pairs that are not in the average structure. Moreover, the splitting of the first PDF peak is absent in the average model but clearly present in the local model.

The local model yields atomic displacements of the Ta and S/Se atoms as they are shown in Fig. 4(c). Shown in Fig. 4(c) is a superposition of the undistorted and locally distorted star lattices. The in-plane differences are due to Ta distortions, which break the local trigonal symmetry. The split of the Ta correlations is also observed in the calculation of the Ta-Ta partial shown in Fig. 4(a) deduced from the local model. The distortions result from in-plane displacement of Ta atoms and out-of-plane displacement of chalcogen atoms. Shown in Fig. 4(e) is the unit cell of the local model that best fits the data. The chalcogen layer is quite distorted, creating quite a multitude of Ta-S and Ta-Se correlations as seen in the partials of Fig. 4(a). From the partials we can deduce that the splitting arises from two types of Ta-S and Ta-Se bonds. Interestingly enough, the splitting is not because of two separate Ta-S and Ta-Se bonds as expected, given that Ta-S bonds and Ta-Se bonds are different in length due to the bigger Se atom. From the partials it can be seen that the Ta-S and Ta-Se correlations are split into two, which indicates that the out-of-plane bonding of Ta with S or Se has at least two bond minima with both S and Se. Details on refinement parameters for the average and local model is given in Supplemental Material [28].

In contrast, the local atomic structure of 1T-TaSe₂ shown in Fig. 4(b) exhibits a somewhat different pattern of distortions in the Ta and Se correlations. First, local correlations responsible for the fitting of the first peak show a broad, single correlation of Ta with Se. This can also be seen from Fig. 4(f) which shows that the chalcogen layer is not as distorted as in TaS₂. Furthermore, multiple pair bonds are present in the Ta-Ta partials, which suggests that the star lattice is locally distorted [Fig. 4(d)] as was previously seen in TaS₂ [22] and also in TaS₂. On the other hand, the Se-Se partial correlation consists of a single peak, which indicates a more uniform chalcogen layer. In contrast, the green solid line corresponding to the average model does not fit the first correlation well and falls short in the 4–5 Å range. Thus, these local distortions are needed to fit the data.

To examine the effect of the CCDW modulations in the local structure, the $G(r)$'s for 1T-TaS₂, TaS₂Se, and TaSe₂ are compared in Fig. 5. Shown in Fig. 5(a) are the data at 2 K, in Fig. 5(b) are the data from 180 K, and in Fig. 5(c) are the data for 300 K. At 2 and 180 K upon warming, TaS₂ and TaSe₂ are in the CCDW state while TaS₂Se is in the NCCDW state. The PDF functions are shifted because the lattice constant expands with Se doping. As described above, all three exhibit Ta in-star and chalcogen out-of-plane distortions. Most distinct are the chalcogen ion distortions in TaS₂Se, which also happens to be superconducting below 3 K as well. At 300 K, TaS₂ is in the NCCDW state just as TaS₂Se is, while TaSe₂ is in the

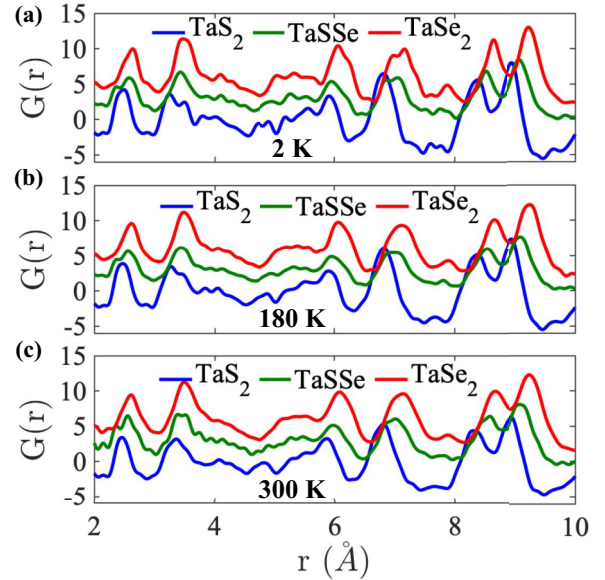


FIG. 5. A comparison of local atomic structure determined from the Fourier transform of the total $S(Q)$ is shown for 1T-TaS₂, TaS₂Se, and TaSe₂. Data are shown at (a) 2 K, (b) 180 K, and (c) 300 K. The $G(r)$ shifts to higher r as the lattice expands with Se doping, as expected. Overall the local structure shows similar features across composition.

CCDW state. It is important to note that very little change is observed across temperature which implies that the set of distortions are present, regardless of the CCDW-NCCDW transitions. Given the absence of any type of stacking order in TaS₂Se and in TaSe₂, we can draw two conclusions from this. First, the absence of a layer stacking order is crucial to the Mott-insulating state of this system. This has a direct effect on the band structure and a gap can open or close based on the stacking. Thus, the absence of stacking in TaS₂Se and TaSe₂ may be linked to their metallic nature.

Second, the chalcogen distortions in TaS₂Se paint a very different picture as to why superconductivity emerges in this system. Previously, it has been assumed that the competition of CCDW and superconductivity is important, and for superconductivity to emerge, CCDW must be suppressed. This is consistent with the appearance of the NCCDW state across the entire temperature range in TaS₂Se. However, *locally*, the atomic structure across the CCDW state to the NCCDW state and back to a CCDW state exhibits the same effects, namely, in-plane Ta distortions in the stars and out-of-plane chalcogen distortions. What is distinctly different in TaS₂Se are the chalcogen distortions. Thus, two scenarios are possible. In one, the chalcogen distortions may be the driver for the suppression of the CCDW state that then makes way for superconductivity. In the other scenario, the chalcogen distortions may actually be the conduit for superconducting pairing.

It is the case that TaSe₂ lacks any kind of stacking order but still shows a CCDW state. The absence of a stacking order is a strong indication as to what happens to the bands, consistent with theoretical predictions [19,20,29]. Moreover, TaSe₂ is metallic. Thus, the appearance of a CCDW state does not automatically open a gap. If that were the case, the

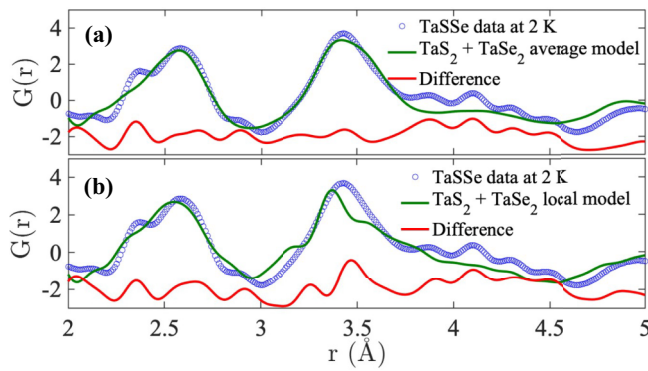


FIG. 6. The experimental neutron PDF data (blue) at 2 K is compared with the calculated PDF (green) based on the model with 50% TaS₂ and 50% TaSe₂. The difference curve is shown in red. The average model is shown in panel (a) and the local model is shown in panel (b).

gap should have appeared around 500 K. Hence, the CCDW transition alone must not be responsible for the insulating behavior of TaS₂. Instead it is the combination of stacking order and out-of-plane orbital ordering that leads to opening of the Mott gap.

To examine the local lattice of TaSSe further, we combined the average and local models determined for TaS₂ and TaSe₂ and compared them to the experimental $G(r)$ of TaSSe at 2 K. The results are shown in Fig. 6. In the experimental data of TaSSe, the first peak shows an inflection that is not well reproduced, neither by the average model nor by the local model shown in Figs. 6(a) and 6(b), respectively. The second major PDF peak corresponds to the Ta-Ta and chalcogen-chalcogen correlations and that is reproduced reasonably well in the average model but not in the local model. The results indicate that TaSSe is not phase separated. Instead a new local order is present which has been linked to the distortions of the

chalcogen layer. Thus the distortion of the chalcogen layer is not simply from the difference in the size of S from Se; hence, the effects are not steric.

To conclude, in TaSSe, significant distortions in the positions of chalcogen atoms were evident, as indicated by peak splitting of Ta-S and Ta-Se correlations. The strong agreement between the experimental PDF and an effective local model, as indicated by the red line in Fig. 4(a), implies that the S and Se out-of-plane local distortions are prominent in this material. The substantial displacement of S and Se atoms is intrinsic to TaSSe and not simply due to variation in the ionic radius between the sulfur and selenium atoms.

At 180 K upon warming, the TaS₂ and TaSe₂ are still in the CCDW state while TaSSe is in the NCDW state. A comparison study of the doping dependence of $G(r)$ is shown in Fig. 5 at temperatures of 2, 180, and 300 K where TaS₂ belongs to the CCDW phase, the CCDW-NCDW boundary, and the NCDW phase, respectively. Particularly interesting is the region $r < 5$ Å. A clear peak splitting was observed at $r \sim 3.3$ Å for TaS₂ in the CCDW phase below 183 K. A detailed investigation of this behavior is reported in Ref. [22]. In the measured temperature range, 2 to 300 K, 1T-TaSe₂ is in the CCDW phase and does not undergo a structural phase transition. This is reflected in the PDF results, where we do not see any significant changes in pair correlations as a function of temperature upon warming [Fig. 3(b)]. The experimental neutron PDF was compared to the calculated PDF based on an average structure model. Differences were observed at the low- r region, which suggests the presence of local distortions.

ACKNOWLEDGMENTS

This work has been supported by the National Science Foundation under Grant No. 2219493. A portion of this research used resources at the Spallation Neutron Source, a DOE Office of Science User Facility operated by Oak Ridge National Laboratory.

- [1] V. Agarwal and K. Chatterjee, Recent advances in the field of transition metal dichalcogenides for biomedical applications, *Nanoscale* **10**, 16365 (2018).
- [2] W. Choi, N. Choudhary, G. H. Han, J. Park, D. Akinwande, and Y. H. Lee, Recent development of two-dimensional transition metal dichalcogenides and their applications, *Mater. Today* **20**, 116 (2017).
- [3] K. S. Novoselov, D. Jiang, F. Schedin, T. J. Booth, V. V. Khotkevich, S. V. Morozov, and A. K. Geim, Two-dimensional atomic crystals, *Proc. Natl. Acad. Sci. USA* **102**, 10451 (2005).
- [4] T. Egami, Y. Petrov, and D. Louca, Lattice effects on charge localization in cuprates, *J. Supercond.* **13**, 709 (2000).
- [5] A. Wegner, J. Zhao, J. Li, J. Yang, A. A. Anikin, G. Karapetrov, K. Esfarjani, D. Louca, and U. Chatterjee, Evidence for pseudo-Jahn-Teller distortions in the charge density wave phase of 1T-TiSe₂, *Phys. Rev. B* **101**, 195145 (2020).
- [6] B. Sipos, A. F. Kusmartseva, A. Akrap, H. Berger, L. Forró, and E. Tutiš, From Mott state to superconductivity in 1T-TaS₂, *Nat. Mater.* **7**, 960 (2008).
- [7] P. Xu, J. O. Piatek, P.-H. Lin, B. Sipos, H. Berger, L. Forró, H. M. Rønnow, and M. Grioni, Superconducting phase in the layered dichalcogenide 1T-TaS₂ upon inhibition of the metal-insulator transition, *Phys. Rev. B* **81**, 172503 (2010).
- [8] L. J. Li, W. J. Lu, X. D. Zhu, L. S. Ling, Z. Qu, and Y. P. Sun, Fe-doping-induced superconductivity in the charge-density-wave system 1T-TaS₂, *Europhys. Lett.* **97**, 67005 (2012).
- [9] J. A. Wilson, F. J. Di Salvo, and S. Mahajan, Charge-density waves in metallic, layered, transition-metal dichalcogenides, *Phys. Rev. Lett.* **32**, 882 (1974).
- [10] K. Sugawara, Y. Nakata, R. Shimizu, P. Han, T. Hitosugi, T. Sato, and T. Takahashi, Unconventional charge-density-wave transition in monolayer 1T-TiSe₂, *ACS Nano* **10**, 1341 (2016).
- [11] P. Chen, W. W. Pai, Y.-H. Chan, A. Takayama, C.-Z. Xu, A. Karn, S. Hasegawa, M.-Y. Chou, S.-K. Mo, A.-V. Fedorov *et al.*, Emergence of charge density waves and a pseudogap in single-layer TiTe₂, *Nat. Commun.* **8**, 516 (2017).

- [12] C. J. Butler, M. Yoshida, T. Hanaguri, and Y. Iwasa, Mottness versus unit-cell doubling as the driver of the insulating state in $1T\text{-TaS}_2$, *Nat. Commun.* **11**, 2477 (2020).
- [13] K. T. Law and P. A. Lee, $1T\text{-TaS}_2$ as a quantum spin liquid, *Proc. Natl. Acad. Sci. USA* **114**, 6996 (2017).
- [14] L. Balents, Spin liquids in frustrated magnets, *Nature (London)* **464**, 199 (2010).
- [15] R. Ang, Z. C. Wang, C. L. Chen, J. Tang, N. Liu, Y. Liu, W. J. Lu, Y. P. Sun, T. Mori, and Y. Ikuhara, Atomistic origin of an ordered superstructure induced superconductivity in layered chalcogenides, *Nat. Commun.* **6**, 6091 (2015).
- [16] A. Spijkerman, J. L. de Boer, A. Meetsma, G. A. Wiegers, and S. van Smaalen, X-ray crystal-structure refinement of the nearly commensurate phase of $1T\text{-TaS}_2$ in $(3 + 2)$ -dimensional superspace, *Phys. Rev. B* **56**, 13757 (1997).
- [17] R. E. Thomson, B. Burk, A. Zettl, and J. Clarke, Scanning tunneling microscopy of the charge-density-wave structure in $1T\text{-TaS}_2$, *Phys. Rev. B* **49**, 16899 (1994).
- [18] P. Fazekas and E. Tosatti, Electrical, structural and magnetic properties of pure and doped $1T\text{-TaS}_2$, *Philos. Mag. B* **39**, 229 (1979).
- [19] T. Ritschel, H. Berger, and J. Geck, Stacking-driven gap formation in layered $1T\text{-TaS}_2$, *Phys. Rev. B* **98**, 195134 (2018).
- [20] T. Ritschel, J. Trinckauf, K. Koepf, B. Büchner, M. V. Zimmermann, H. Berger, Y. I. Joe, P. Abbamonte, and J. Geck, Orbital textures and charge density waves in transition metal dichalcogenides, *Nat. Phys.* **11**, 328 (2015).
- [21] Y. Liu, R. Ang, W. J. Lu, W. H. Song, L. J. Li, and Y. P. Sun, Superconductivity induced by se-doping in layered charge-density-wave system $1T\text{-TaS}_{2-x}\text{Se}_x$, *Appl. Phys. Lett.* **102**, 192602 (2013).
- [22] S. S. Philip, J. C. Neuefeind, M. B. Stone, and D. Louca, Local structure anomaly with the charge ordering transition of $1T\text{-TaS}_2$, *Phys. Rev. B* **107**, 184109 (2023).
- [23] B. H. Toby, *EXPGUI*, a graphical user interface for *GSAS*, *J. Appl. Crystallogr.* **34**, 210 (2001).
- [24] B. E. Warren, *X-Ray Diffraction* (Courier Corporation, North Chelmsford, Massachusetts, 1990).
- [25] T. Egami and S. J. L. Billinge, *Underneath the Bragg Peaks: Structural Analysis of Complex Materials* (Elsevier, Amsterdam, 2003).
- [26] V. Petkov, J. E. Peralta, B. Aoun, and Y. Ren, Atomic structure and Mott nature of the insulating charge density wave phase of $1T\text{-TaS}_2$, *J. Phys.: Condens. Matter* **34**, 345401 (2022).
- [27] S. S. Philip, D. Louca, J. C. Neuefeind, M. B. Stone, and A. I. Kolesnikov, Suppression of stacking order with doping in $1T\text{-TaS}_{2-x}\text{Se}_x$, *Condens. Matter* **8**, 89 (2023).
- [28] See Supplemental Material at <http://link.aps.org/supplemental/10.1103/PhysRevB.109.094118> for further details including the calculated PDF at longer r range and refinement details.
- [29] K. Rossnagel, On the origin of charge-density waves in select layered transition-metal dichalcogenides, *J. Phys.: Condens. Matter* **23**, 213001 (2011).